Research article

PREOPERATIVE AND INTRAOPERATIVE CT IMAGING FOR ORBITAL FOREIGN BODIES IDENTIFICATION AND SURGICAL PLANNING IN VETERINARY MEDICINE

Siniša D. GROZDANIĆ[1,2,3*] , Heidi MURTHA[1], Tatjana LAZIĆ [1,2,3],
Slavica ĐUKIĆ[2], Sergei LUZETSKII[2], Daniel C. URSU[4], David SARMENT[4]

[1]Animal Eye Consultants of Iowa, Hiawatha, IA 52233; [2]Oculus Veterinary Clinic, Belgrade,11000, Serbia; [3]TL VetPath International Consultants, Hiawatha, IA 52233; [4]Xoran Technologies LLC, Ann Arbor, MI 48108.

The goal of this study was to evaluate sensitivity of intraoperative Computed Tomography (iCT) imaging for the detection of orbital foreign bodies (OFBs) in an *in vitro* model and evaluate iCT efficacy for surgical planning of OFB detection and removal in veterinary patients. Three canine patients were presented to our hospital for potential orbital foreign body removal. *In vitro* studies were conducted using a canine skull model with placement of various OFBs. Four different examiners utilized CT imaging to evaluate the detection of OFBs. A surgical navigation system was employed to assess the feasibility of stereotactic orbital foreign body retrieval *in vitro*. iCT imaging was applied for surgical planning and guidance of orbital surgery for the removal of OFBs in three clinical patients. *In vitro* experiments revealed a high detection rate for objects with high radiopacity such as metal and glass. The detection rate for organic foreign bodies such as wood was moderate, while for plastic foreign bodies ranged from moderate to low. Navigation was successfully used for OFB retrieval. iCT was effectively employed for detecting OFBs in clinical patients. However, porcupine quills were better detected using standard ultrasound imaging. The use of iCT potentially represents an evolving technological practice that enables real-time imaging to improve the precision of surgical procedures.

Keywords: Computed Tomography, orbit, foreign body, surgery

INTRODUCTION

Intraoperative computed tomography (iCT) is an advanced modality that allows for real-time, high-resolution imaging of the orbital structures during surgical procedures. This technology significantly improves the accuracy, safety, and effectiveness of orbital

---

*Corresponding author: e-mail: sgrozdanic@animal-eye-iowa.com

surgery by providing immediate visualization of the operative field. This ability allows surgeons to make adjustments and confirm the success of their interventions [1,2].

ICT imaging offers major advantages over traditional preoperative imaging. Real-time visualization with iCT can be rapidly acquired during surgery, providing up-to-date information about the position and status of the orbital structures, while ensuring that the surgical plan remains accurate and relevant [1-3]. By offering better visualization of critical structures such as the optic nerve, extraocular muscles, and blood vessels, iCT contributes to minimizing the risk of inadvertent damage during surgery, and allows for a more precise approach toward the foreign body/tumor retrieval, considering a possibility of the structural dislocation, which can develop as a result of tissue manipulation [1,4,5]. Furthermore, intraoperative imaging can confirm the successful removal or manipulation of target tissues, enabling the surgeon to immediately address any issues, thereby reducing the likelihood of reoperations or surgical failure of the primary procedure [2,3,6].

Applications of iCT orbital imaging has been traditionally utilized to ensure complete removal of orbital tumors while minimizing damage to surrounding structures [2]; for confirmation of the exact location and orientation of an orbital foreign body to streamline the retrieval process and reduce the risk of complications [7-9]; reconstruction surgery to guide the proper placement of implants and prosthetic devices, ensuring optimal positioning and outcomes [1,3]; and for orbital decompression surgery to guide the surgeon in alleviating the causes for the compressive injury with a goal of improving the surgical outcomes and restoring the normal vision [10,11].

Despite the many advantages of iCT imaging, there are some challenges and limitations. The cost of acquisition and maintenance of the equipment can be expensive; obtaining intraoperative images during surgery may increase the duration of the procedure, potentially resulting in a longer anesthesia time and increased expenses; as with any CT imaging, there is an increased risk of radiation exposure for both the patient and surgical team dictating the need for the organizational measures to minimize radiation exposure to humans and animals.

This article discusses the advantages, and challenges associated with the use of preoperative, intraoperative and postoperative CT imaging used for orbital foreign body (OFB) surgeries in veterinary patients through a selection of clinical cases evaluated and operated at the Animal Eye Consultants of Iowa in the period of 2020-2023. This article discusses possible future technological developments toward minimally invasive stereotaxic surgeries.

MATERIAL AND METHODS

In vitro studies

Foreign Bodies

Four different materials – metal, wood, plastic, and glass were used as OFBs in this *in vitro* study.

Specimens

A commercially available canine skull (Lake Forest Anatomicals, Lake Forest, IL) retrofitted with porcine eyes, periocular skin and periorbital soft tissue (Animal Technologies, Tyler, TX), was used as an *in vitro* model for OFB placement and imaging (Figure 1). A total of nine clinical scenarios were simulated in a randomized and masked manner (Table 1). The skull was placed in a container and immersed in water to approximate the volume of a head soft tissue in order to provide similar x-ray attenuation. The location and type of the foreign body were not known to the examiners who reviewed CT images. The experiment also contained the control skull specimen which did not contain any foreign bodies.
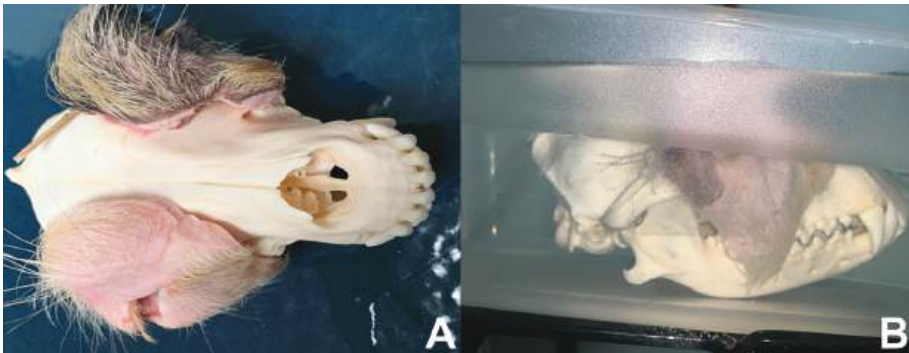

Figure 1. *In vitro* model used for the foreign body detection in this study. **(A)** Canine skull equipped with pig eyes and periocular skin tissue; **(B)** The model is immersed in a plastic container with water prior to and during imaging.

Table 1. Detection scores for the *in vitro* study. Metal and glass OFBs had the highest detection scores, followed by polycard plastic and large wood OFBs. Styrene plastic and wood OFBs with a small diameter had the lowest detection score or were not detectable at all. **OD** – right eye; **OS** – left eye

Foreign Object	Eye	Detection score experienced	Detection score novice	Object dimensions (mm)
BB bullet (lead) – case 1	OS	4	4	2.5x2.5
Plastic – Polycarbonate – case 2	OS	3	0	10x4
Metal pin – case 3	OS	4	4	27x2
Wood Stick + metal pin – case 4	OS	2/4	0/4	38x4/27x2
Wood Stick – case 5	OS	0	0	18x2
Glass – case 6	OD	4	4	7x5
Plastic – Styrene – case 7	OD	0	0	11x5
Wood stick – case 8	OD	3	0	96x5
No Foreign Body – case 9	N/A	false detection of wood foreign body assigned (grade 2)	0	N/A

A dog skull equipped with fiduciary markers and draped to conceal the location of the inserted foreign bodies, was used for the stereotaxic image navigation and foreign body retrieval procedures (Figure 2).
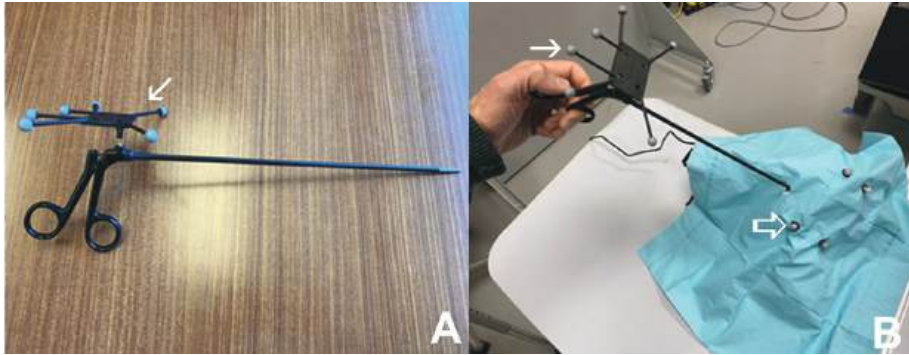
Figure 2. *In vitro* model used for the prototype stereotaxic navigation foreign body retrieval experiments. **(A)** Long orbital forceps with stereotaxic navigation markers (white arrow); **(B)** The model of the canine skull with the placement of head stereotaxic fiduciaries (open arrow) and sterile draping for the stereotaxic surgery.

Imaging

Cone-beam CT (CBCT) imaging

CBCT scanning was performed using VetCatIQ (foreign body detection study, *in vivo* studies) and vTron (stereotaxic surgery studies) units (Xoran Technologies, Ann Arbor, Michigan). A 20-second, 600 frame, 360 degrees acquisition, using a flat panel 40x30cm detector, was reconstructed at a 0.3mm isotropic slice thickness using a standard FDK (Feldkamp Davis Kress) reconstruction algorithm.

Analysis

A previously described scoring scale ranging from 0 to +4 was used for assessing visibility of OFBs (Table 2) by four different examiners [12,13]. The examiners were not aware of the type and position of OFBs. Two of the examiners were considered novices (SD, SL), while the other two were experienced, each with nearly twenty years of experience in terms of the CT image evaluation (SG, DS)

The observers were unaware of the composition, location or the number of OFBs on images. Post analysis of the position of OFBs, which were not correctly detected on initial images, was performed placing a metal needle as a fiduciary marker in the foreign body, and repeating the CT.

Table 2. Four-point scoring scale for OFB detection and image interpretation [13]

Score	Quality	Definition
+4	Excellent	Excellent resolution of details and excellent visibility, good demarcation from surroundings
+3	Good	Good resolution of details, demarcation from surroundings, clear visibility
+2	Fair	Insufficient resolution of details, insufficient visibility, insufficient demarcation
+1	Bad	Details not resolved, bad demarcation from surroundings, bad visibility
0	No image	Invisible

Sterotaxic Surgical Navigation

Navigation

An experimental augmented-reality navigation system was developed to simulate CT-image guided surgical interventions. The system was primarily composed of commercially available hardware components: an optical tracking system employing passive infrared reflective optical tracking markers (OptiTrack, NaturalPoint, Inc. Corvallis, OR) and a surgical laparascopic grasper (Symmetry Surgical, Antioch, TN). Reflective markers were rigidly mounted to the laparoscopic grasper tool, and a plastic model of a canine skull (Skulls Unlimited, Oklahoma City, OK), which served as the simulated patient. The presence of a foreign object in the inferior right ocular orbit was simulated by placing a small wooden splinter into sculpting clay which served to semi-rigidly attach it to the canine skull model.

Three-dimensional rendering and real-time tool representation were provided during the simulated biopsy procedure as follows. CT-image data was transferred to a software platform (Xoran Technologies, Ann Arbor, Michigan) and tool navigation was rendered on a multi-planar reconstruction viewer. Paired-point patient registration was used to correlate the location of the optical markers in the CT image space and real-world space. The spatial relationship between the laparoscopic tool and canine model was calculated in real-time based on the rigid-body coordinates supplied by the optical tracking system. This relationship was then transformed into CT image space to facilitate the overlay of a virtual rendering of the laparoscopic tool onto the CT-scan

of the canine skull model. A total of six repetitions with different locations of OFB has been done to test the accuracy of the approach.

Figure 3. Patient positioning for intraoperative imaging. **(A)** The CT imaging holder is fixed to the operating table and patient is positioned for preoperative CT imaging; **(B)** A sterile drape is positioned over the patient and fixed with sterile surgical tape to prevent contamination of the drape and field during the imaging. Towel clamps have to be temporarily removed during imaging to eliminate the metallic shadow artifacts, so proper positioning of sterile tapes becomes essential for keeping the surgical drape in position.

In vivo studies

All studies were conducted in accordance with the ARVO Statement for Use of Animals in Ophthalmic and Vision Research and in compliance with GERVO policy. All diagnostic and surgical procedures were approved by clients pursuing treatment at the Animal Eye Consultants of Iowa who provided a signed consent form for diagnostic and treatment options, and possible risks and complications. A total of 3 canine clinical patients with different forms of orbital foreign bodies (Table 3) were evaluated and treated in the period between January 2020 and June 2023. Patients were from three US states (North Dakota, Iowa, Michigen), and were diagnosed with OFBs by two different ophthalmologists.

All patients received a complete ophthalmic examination: slit lamp biomicroscopy, indirect ophthalmoscopy, tear production and intraocular pressure evaluation, and basic neuro-ophthalmology evaluation (palpebral and corneal reflex, ocular motility

evaluation). Menace, dazzle, and chromatic pupil light reflexes were performed to evaluate the status of the visual system. Full laboratory evaluation (complete cell blood count, serum chemistry, urine analysis +/ – pancreatitis test) was performed for all patients. CT imaging and surgical procedures were performed under general anesthesia and with the standard postoperative use of systemic antibiotics, anti-inflammatory and pain medications pertinent to the type of procedure.

Table 3. Detection scores for the *in vivo* study patients. Board certified radiologists had a higher detection failure rate compared to the board certified ophthalmologist intimately involved with the cases. **OS** – left eye; **US** – ultrasound

Patient	Pathology	Eye	Detection score	Radiologist detection	Ophthalmo-logist detection
Labrador Retriever, 2y, F	Orbital foreign body (wood)	OS	2	0	YES
German Shorthaired Pointer, 6Y, SF	Orbital foreign body (porcupine quills)	OS	2	one detected, one missed on CT	one detected, one missed on CT, intraoperative detection with US – 2 foreign bodies
Boston Terrier, 3Y, CM	Orbital foreign body (silicone oil)	OS	3	0	YES

RESULTS

In vitro studies

Orbital Foreign Body Detection Using the CT

In vitro studies revealed the high accuracy for the detection of OFBs with a strong radiopacity (metal, glass) by experienced and novice evaluators, while reliable detection of wood and plastic foreign bodies had mixed results (Table 1). Canine skull fitted with porcine eyes and periocular soft tissue, and immersed in the water provided a realistic *in vitro* model for the evaluation of OFBs (Figure 1, 4-10). Experienced examiners provided much better accuracy compared to novice examiners for OFBs with lower radiopacity, while some OFBs were not detected at all, confirming the limitation of CT technology for organic material OFBs detection.
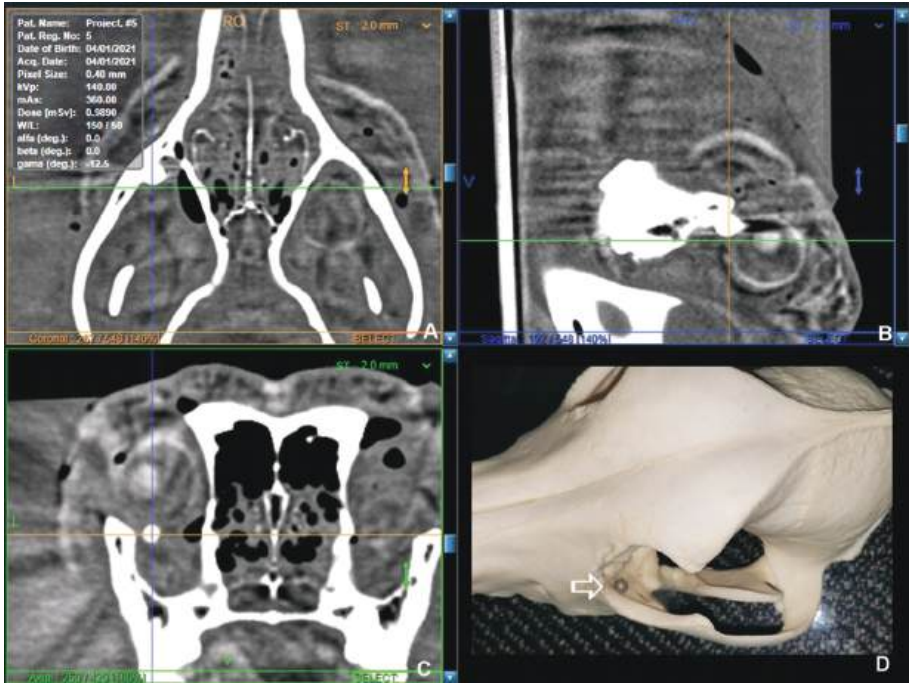
Figure 4. Case 1. Detection of a round metal foreign body (gunshot pellet) in the in vitro skull model. Metal foreign body is clearly identified on all CT sections – coronal **(A)**, sagittal **(B)** and axial **(C)** - metal foreign body is marked by a crosshair pointer. The axial view has the best visibility of the metalic object, and some star-like radiating shadow patterns are visible, typical of metal foreign objects. **D)** The metal foreign body was taped to the canine skull model in the ventro-cranial orbital space (arrow) prior to placement of soft tissue components.
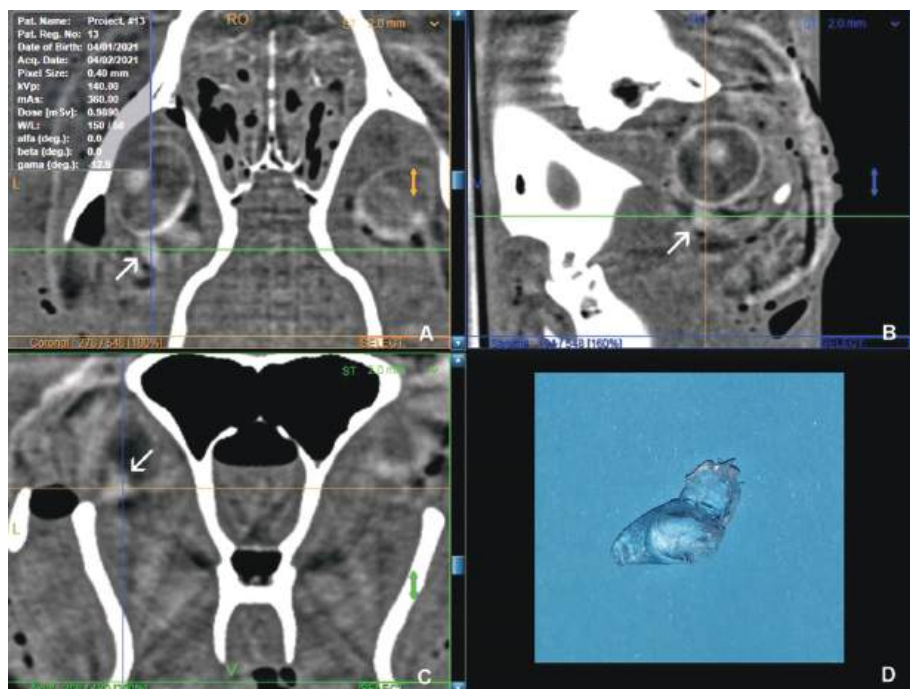
Figure 5. Case 2. Detection of a plastic foreign body (polycarbonate fragment) in the in vitro skull model. A plastic foreign body is identified on axial **(A)**, sagittal **(B)** and coronal **(C)** CT sections (arrows). However, radiopacity is very similar to the scleral tissue. **D)** Polycarbonate fragment prior to placement in the orbit..
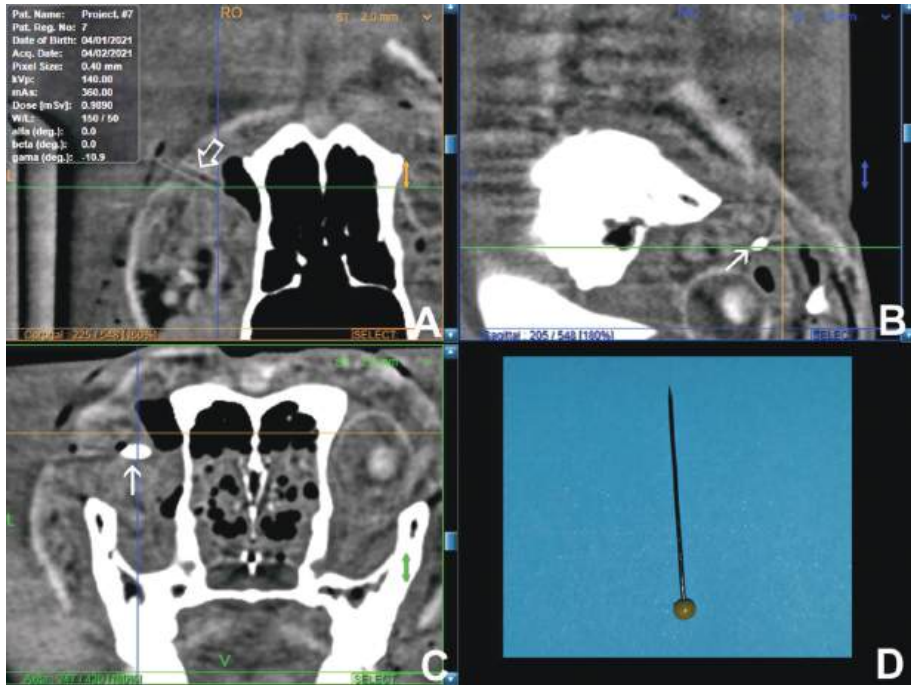
Figure 6. Case 3. Detection of the linear metal foreign body (metal pushpin) in the *in vitro* skull model. A metal foreign body is identified on sagittal and axial (images **B** and **C** – closed arrow) CT sections. The coronal section reveals the presence of the metal shadow artifact, which can be mistaken for a wood or plastic foreign body (image **A** – open arrow).
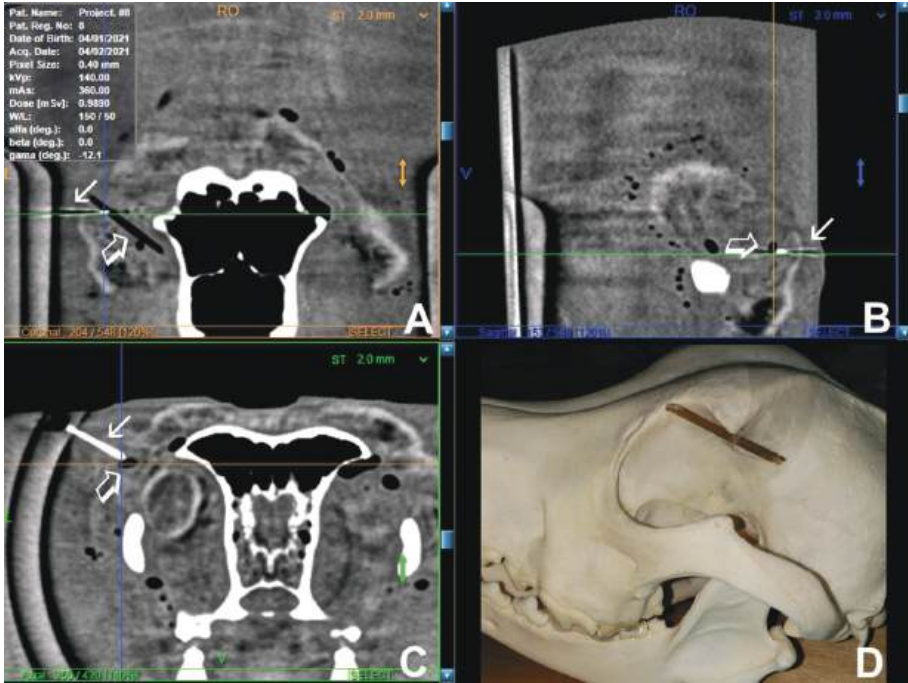
Figure 7. Case 4. Detection of the wood and metal foreign body in the in vitro skull model. **A)** Coronal view – the open arrow points to the linear profile with decreased radio opacity similar to air, which can be observed with organic material foreign bodies with the lower density and higher air content, the closed arrow points to the stainless steel needle shadow artifact (metal foreign body) which was imbedded in the soft tissue in the close proximity to the wood foreign body; **B)** Sagital view reveals a much smaller profile of both foreign bodies; **C)** Axial view reveals much better location and intensity of the metal foreign body; **D)** Photograph of the skull with taped wood foreign body..
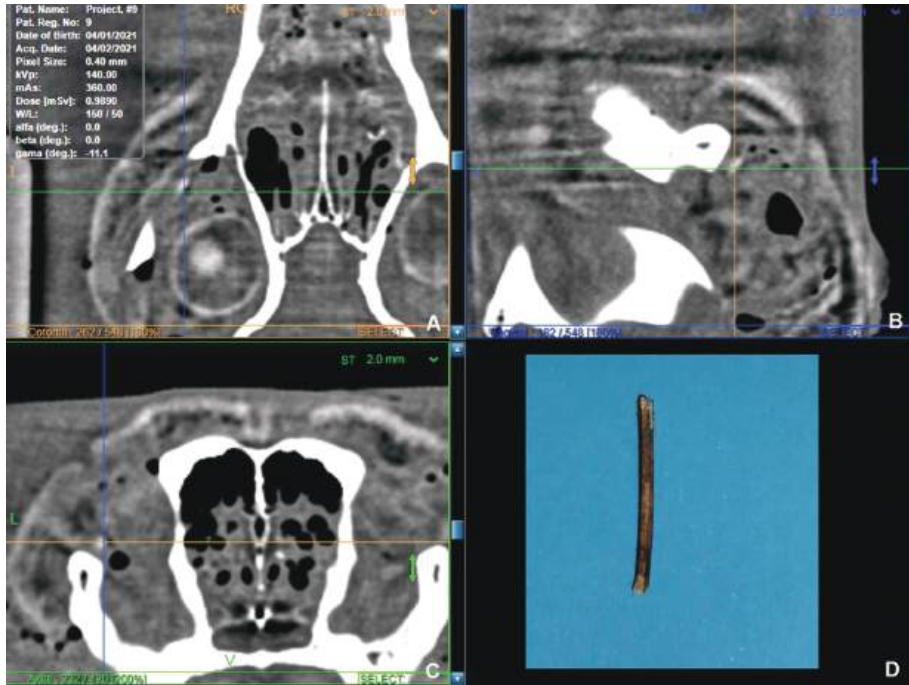
Figure 8. Case 5. Detection of the wood foreign body embedded in soft tissue in the in vitro skull model. In this particular scenario, examiners did not detect the presence of the foreign body, and images were read as normal in coronal **(A)**, sagittal **(B)** and axial **(C)** views. Additional metal fiduciary was placed next to the foreign body (crossline over the small object with increased radiodensity) to help with the identification of the foreign body position in the secondary scan. **D)** The image of the wood foreign body before placement in the orbit.
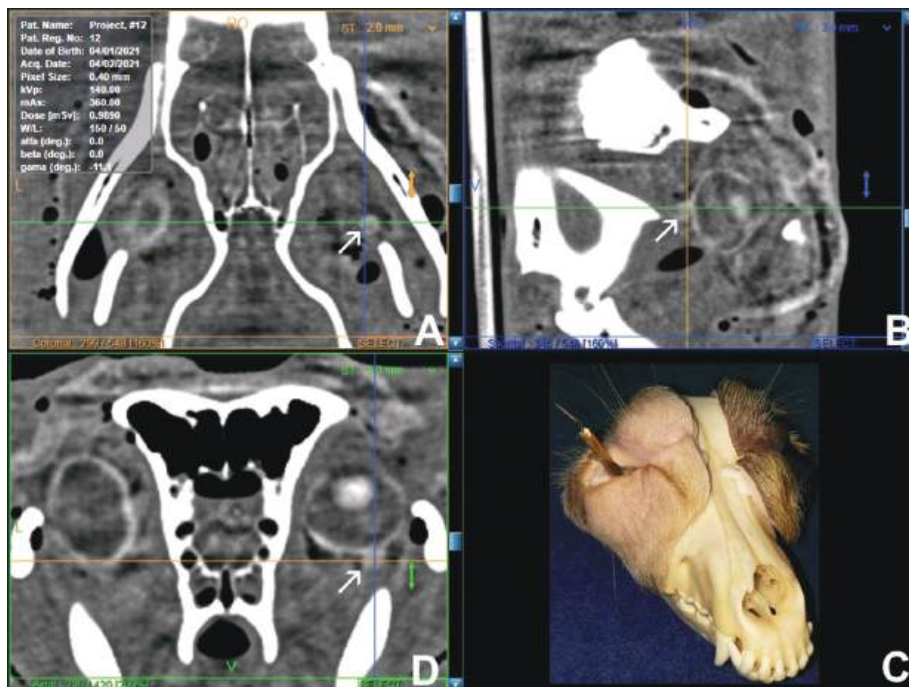
Figure 9. Case 8. Detection of the wood foreign body embedded in soft tissue in the in vitro skull model. **A)** Coronal view – the arrow points to the round foreign body profile with increased radio opacity similar to scleral tissue, **B)** Sagital view reveals a position of the foreign body in the close proximity to the eye globe (arrow); **C)** Axial view reveals a position of the foreign body in the close proximity to the eye globe; **D)** Photograph of the skull with the wood foreign body inserted in the soft tissue.
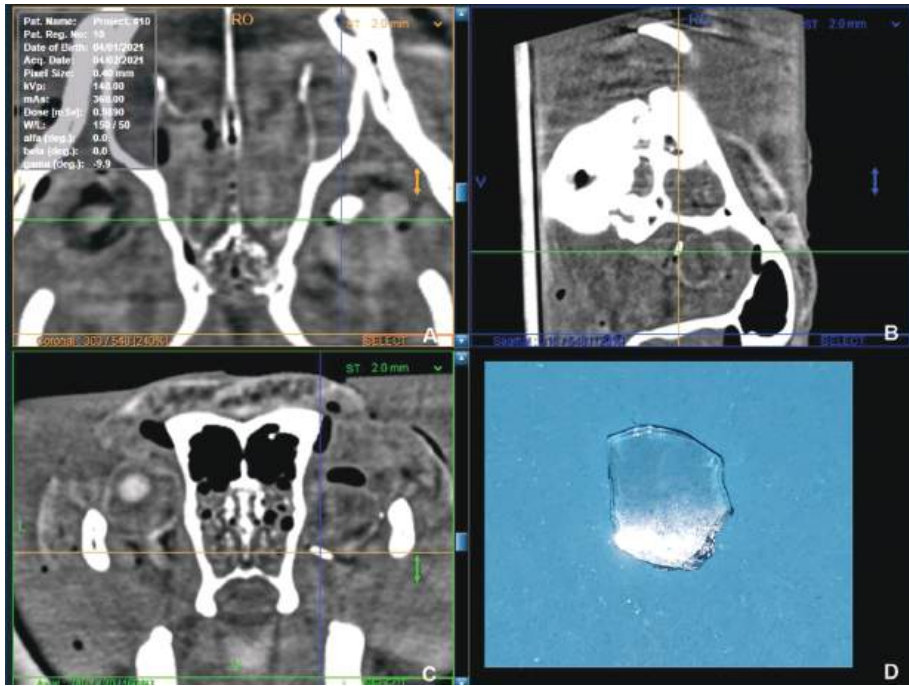
Figure 10. Case 6. Detection of the flat glass foreign body in the in vitro skull model. Glass foreign body is clearly identified on coronal **(A)**, sagittal **(B)** and axial **(C)** CT sections (crosshair pointer) as an object with the high radiopacity. **D)** The image of the glass foreign object before placement in the orbit.

Orbital Foreign Body Detection and Retrieval Using the Stereotaxic Navigation Approach

Three-dimensional rendering and real-time tool representation was successfully achieved during the simulated OFB retrieval in all attempts (Figure 11). The retrieval of small objects requires good hand-eye coordination, and with additional attempts the procedure was faster and smoother. Combination of the retrieval tool with the stereotaxic guided endoscopic tool will likely provide much better and faster results in terms of the object retrieval due to the dual visual control of the OFB location.

Patient Study

Detection scores for the *in vivo* study patients showed lower performance by board certified radiologists compared to the board certified ophthalmologist intimately involved with the cases (Table 3).
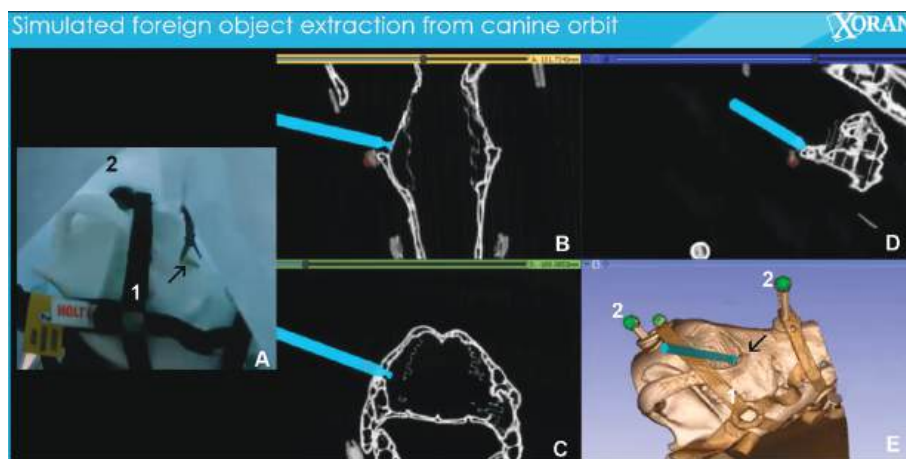
Figure 11. Sterotaxic navigation approach. **(A)** A canine skull model equipped with the strap **(1)** holding fiduciaries **(2)** for location detection is combined with CT imaging to generate the precise map for different orbital structures and localization of the wood foreign body (arrow). **(A)** Coronal view – the blue object is a digital representation of the grasping forceps approaching the wood foreign body in the coronal **(B)**, axial **(C)** and sagittal **(D)** view. Three-dimensional live image reconstruction is available for the more precise positioning of the retrieval instrument in real-time **(E)**.

Clinical Case 1

The patient presented with a history of intermittent mucopurulent discharge from the right eye for 2 months. Three months prior had a hunting accident where a piece of the wood stick was found in ventral conjunctiva and removed by a local veterinarian. On ophthalmology examination there was no evidence of ocular discomfort or redness, just the presence of a mucopurulent discharge was evident at the right medial canthus (Figure 12). Intraocular pressure (IOPs) and tear production (STT) were normal. The patient had normal ocular motility and retropulsion, there was no pain present during the retropulsion or mouth opening. Nasolacrimal duct flush was performed, which revealed normal duct patency and absence of discharge coming from nasolacrimal punctae or nasal cavity. There was a limited mobility of the third eyelid, but there was no evidence of foreign bodies behind the nictitans before and after the extensive saline flush was performed. The rest of the ophthalmology and general physical examination was unremarkable. Due to the previous history of wood foreign body, there was a concern that a possible orbital remnant of the foreign body may be responsible for the observed changes so ultrasound and CT imaging with explorative minimally invasive endoscopic orbital surgery was proposed. Ultrasound imaging was declined, due to the perceived inferior diagnostic capability compared to CT imaging. The patient was routinely anesthetized, surgically prepped and moved in the operating room. Intraoperative CT imaging was performed which revealed the possible presence of the orbital foreign body in the ventral orbit (Figure 12).
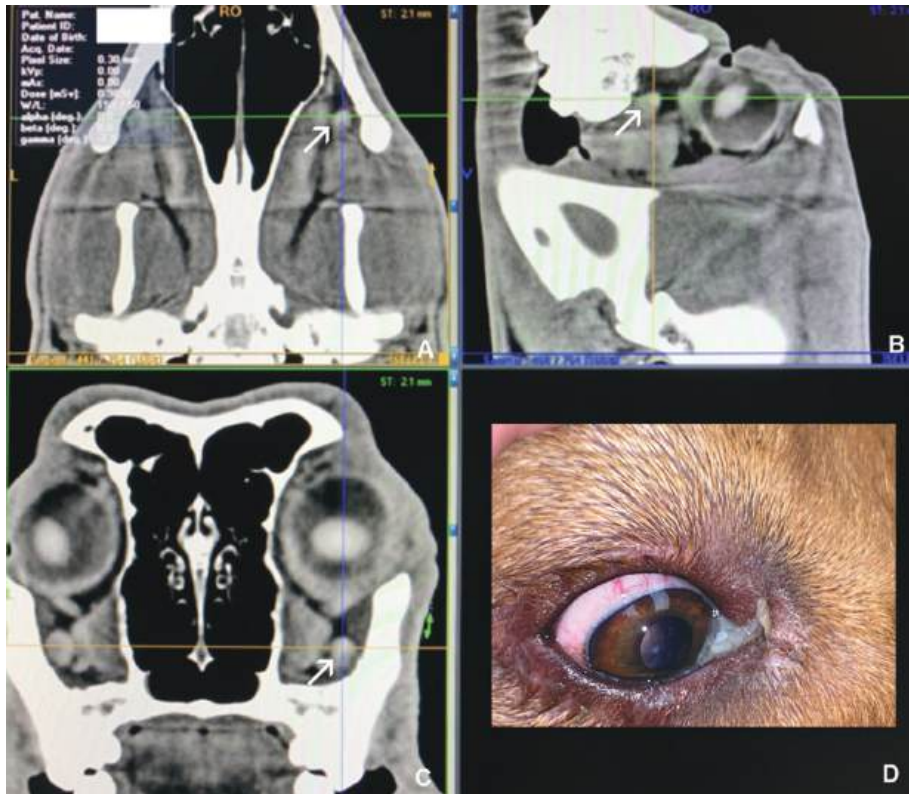
Figure 12. Clinical case 1. Detection of the wood foreign body in the ventral orbital space. Wood foreign body was identified in the coronal **(A)**, sagittal **(B)** and axial **(C)** all CT sections (arrow) as an object with the soft tissue radioopacity. **(D)** Clinical appearance of the patient at the time of examination revealed comfortable and non-inflamed eye with mild mucopurulent discharge.

The third eyelid was retracted and Stevens tenotomy scissors were used to make a ventral conjunctival incision (10 mm long). Upon the ventral conjunctiva's opening, a drainage tract was identified with hemorrhagic content. A bacteriology sample was submitted for aerobic and anaerobic culture and sensitivity, and the tract was flushed and explored using the alligator forceps. The micro alligator forceps was introduced to the ventral orbital space to the depth where CT imaging revealed the possible presence of a foreign body, which expanded the drainage tract and allowed for the visualization of the top part of the foreign body. The foreign body was gently grasped to avoid the loss of any fragments and retrieved from the orbital space (Figure 13). Orbital endoscope was not utilized for this surgical procedure, due to the early identification of the OFB without endoscopic help. The drainage tract was left open, and standard postoperative therapy was initiated using oral enrofloxacin (8 mg/kg BW q24h for 14 days, Dechra, Overland Park, KS), carprofen (Rimadyl, 2.2 mg/kg BW q12h for 14 days, Zoetis, Parsippany, NJ) and triple antibiotic ointment (Neopolybac QID OD,

Bausch and Lomb, Vaughan, ON, CA). An E-collar was provided for the period of 7 days and limitation to physical activity was recommended for a period of 7 days (leash walks only). Microbial analysis revealed the presence of *Staph. epidermidis* susceptible to enrofloxacin.

The recheck evaluation with the local veterinarian 14 days after the procedure revealed complete resolution of the mucopurulent discharge and a comfortable eye appearance.
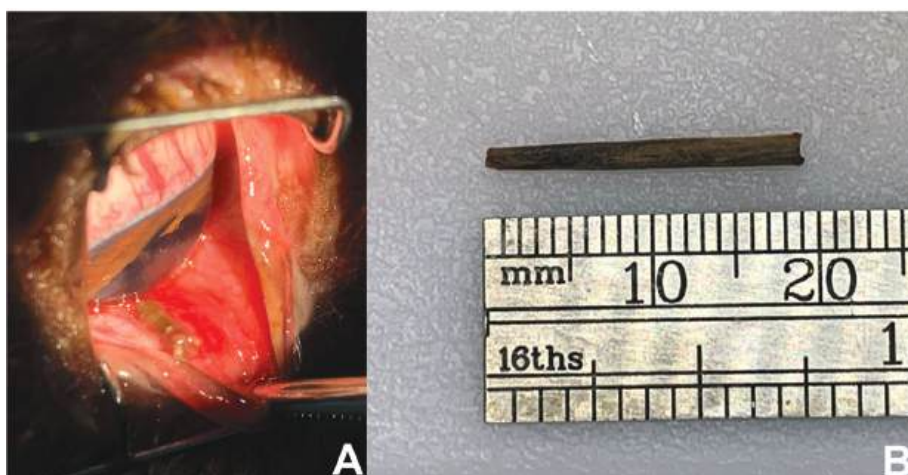

Figure 13. Clinical case 1. (A) Intraoperative image of the foreign body retrieval from the ventral orbital space. **(B)**. Wood foreign body (20x3 mm) was retrieved in the single piece and without fragmentation from the ventral orbital space.

Clinical Case 2.

The patient presented with a history of the porcupine encounter three weeks prior which resulted in the removal of 30-40 porcupine quills from the upper left lip. One week after the procedure for the removal of porcupine quills, the left eye developed ocular discomfort on palpation, retropulsion and mouth opening, with clinical signs of enophthalmos and elevated third eyelid. Systemic antibiotics (amoxicillin and clavamox) were prescribed in combination with carprofen by the local veterinarian. Two board-certified ophthalmologists in the local specialty center, established the diagnosis of a possible presence of an orbital porcupine quill using ultrasound and CT imaging. The foreign body was located in the close proximity to the optic nerve and resulted in the indentation of the ventral medial fundus quadrant resulting in the retrobulbar mass/structure pressure on the eye globe. The initial plan by a local ophthalmologist was to pursue a lateral zygomatic orbitotomy in collaboration with the board-certified surgeon, however, there was a concern that the medial positioning of the foreign body may limit the accessibility via lateral approach. Furthermore, there was a concern that the proximity of the quill to the optic nerve and sclera may result in an intraoperative penetrating injury to the eye globe or optic nerve. A referring

ophthalmologist contacted our institution to discuss a referral for endoscopic orbital surgery. The plan was to pursue medial endoscopic approach with the goal of removing the foreign body from the medial side, which should have decreased the risk of the foreign body migration and possible iatrogenic injury to sensitive ocular structures. Upon ophthalmological examination at our institution, both eyes were visual and comfortably open. There was an enophthalmos and nictitans elevation present in the left eye. Fundus evaluation revealed indentation of the ventral nasal quadrant. Retropulsion was not pursued due to the concerns of possible foreign body migration and iatrogenic choroidal/retinal penetration injury based on the previous evaluation of the ultrasound and CT images from the referring institution. Ophthalmic ultrasound was pursued using the 10 and 20 MHz probes (Reichert Inc, Buffalo, NY), and it revealed the existence of an orbital abscess formation with the presence of a foreign body in very close proximity to the optic nerve and sclera (Figure 14,15). The plan was made to pursue iCT imaging combined with endoscopic orbital surgery, followed by control intraoperative ultrasound and additional iCT imaging to confirm the successful removal of the foreign body.
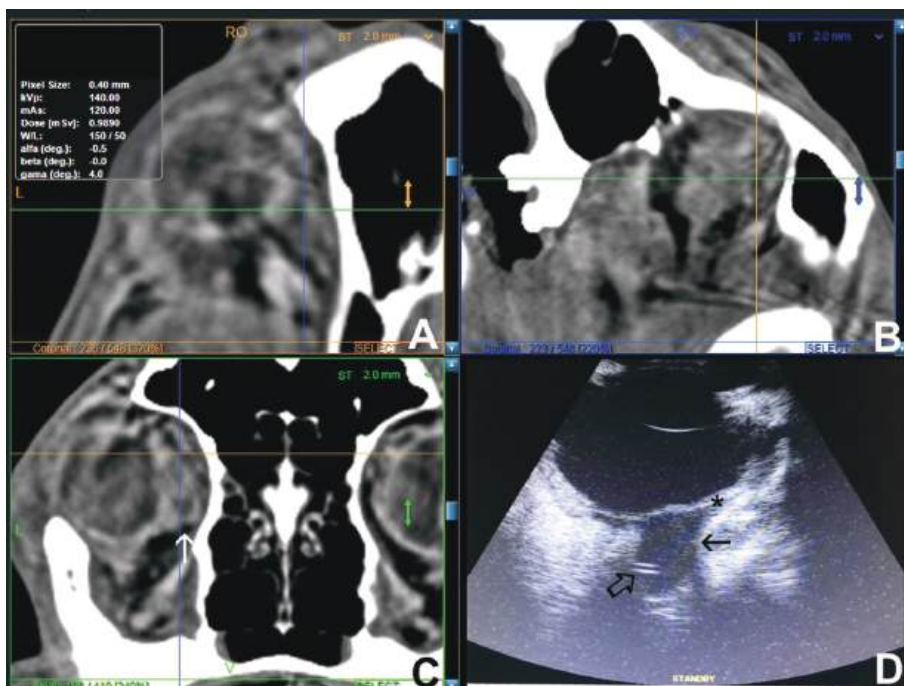

Figure 14. Clinical case 2. Preoperative CT and ultrasound imaging for the case number 2. **(A)** Coronal section did not reveal a clear position of the foreign body, while sagittal **(B)** and axial sections **(C)** revealed a linear tract with the low radiopacity (cross section of the marker lines) indicative of the foreign body opacity. The arrow in the image C points to the abscess formation **(D)**. Preoperative ultrasound revealed abscess formation (closed arrow) with a foreign body imbedded in the abscess region (open arrow). The abscess is compressing and indenting sclera (star).

The patient was routinely anesthetized, standardly prepared for surgery and positioned in the operating room. An iCT imaging was performed to confirm the location of the foreign body prior to the start of surgery (Figure 14). A betadine soaked gauze was placed in the oral cavity and a 15 blade was used to create the incision behind the last molar on the left side. The incision was bluntly extended to the orbital cavity using Mosquito hemostats with the goal to help with the drainage of blood and possible inflammatory material during the orbital surgery and reduce the risk of compressive optic neuropathy in the postoperative period.
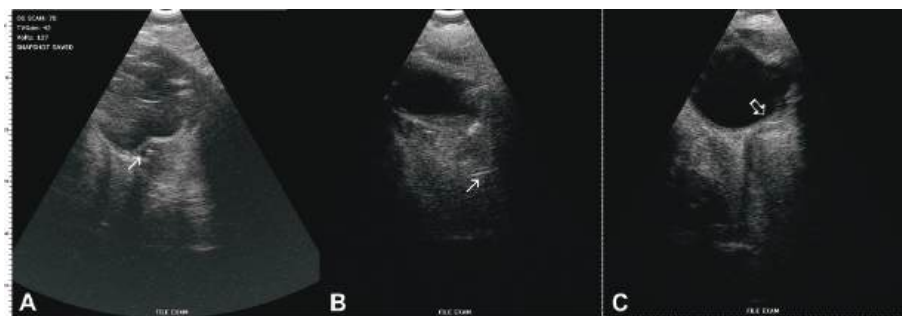

Figure 15. Clinical case 2. (A) Preoperative ultrasound revealed an OFB (arrow) near the optic nerve and sclera with the indentation of the eye globe, creating the risk for the imminent perforation of the eye globe. **(B)** Intraoperative ultrasound after the retrieval of the first OFB identified the second OFB (arrow) in the deep orbital space (not detected on multiple preoperative CT scans). **(C)** Control intraoperative ultrasound after the removal of both OFBs revealed resolution of the eye globe indentation (open arrow).

A lateral canthotomy was performed using Mayo scissors. A 300-degree conjunctival peritomy was performed using Wescott tenotomy scissors. The dorsal and lateral rectus muscles were isolated using the Gass retinal hook and tied up using 6-0 Vicryl to allow for the manipulation of the eye globe. Blunt dissection of the orbital tissue was performed by means of Mosquito hemostats. Orbital depressors were used to manipulate the orbital tissue and globe so a 19g curved endoscopic probe (Endo Optiks, BVI, Waltham, MA) could be introduced in the orbit for the orbital inspection and retrieval of the orbital foreign body (Figure 16,17).
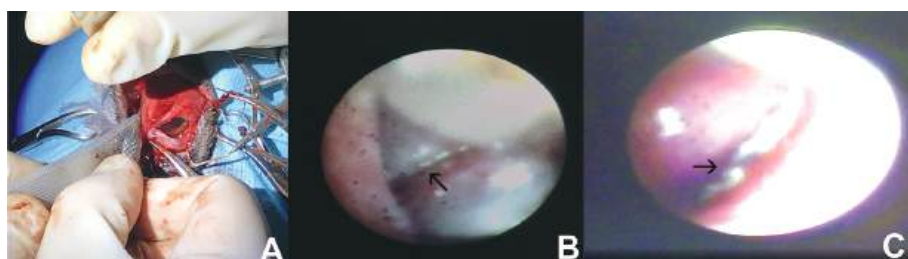

Figure 16. Clinical case 2. (A) Intraoperative image of the orbital endoscopy with the use of 19g curved Endoptiks probe. An assistant is retracting the eye globe and orbital soft tissue using the blunt orbital depressors to allow for better visibility of the orbital space. **(B)** The first porcupine quill was identified close to the eye globe. **(C)** The second porcupine quill was endoscopically identified in the deep portion of the ventral orbit.

The first orbital foreign body was identified using the endoscope and carefully retrieved using the alligator forceps under endoscopic guidance (Figure 16,17).

Figure 17. Clinical case 2. (A) Conjunctival peritomy (360 degrees) was performed with the placement of the stay sutures around rectus muscles for the manipulation of the eye globe. **(B)** Intraoperative ultrasound imaging was performed with ultrasound gel placed inside the sterile sleeve. **(C)** Porcupine quill retrieval from the orbit. **(D)** Two porcupine quills retrieved from the orbit (15-18 mm length, 1-2 mm width).

A bacterial culture sample was collected but it did not reveal aerobic or anaerobic growth (suspect due to the extensive blood presence in the orbit at the time of

sample collection). A control intraoperative ultrasound was repeated, which identified a second orbital foreign body in the deep ventral orbital space (Figure 15), which was endoscopically identified and retrieved from the orbit (Figure 16,17). Additional intraoperative ultrasound (Figure 15) and iCT imaging (Figure 18) was pursued to confirm that no additional orbital bodies were present, and the abscess was drained and thereof it did not compress the eye globe anymore. Conjunctival tissue was closed using the 6-0 Vicryl absorbable suture. Lateral canthotomy was closed using the 5-0 PGA absorbable suture (Figure 18).
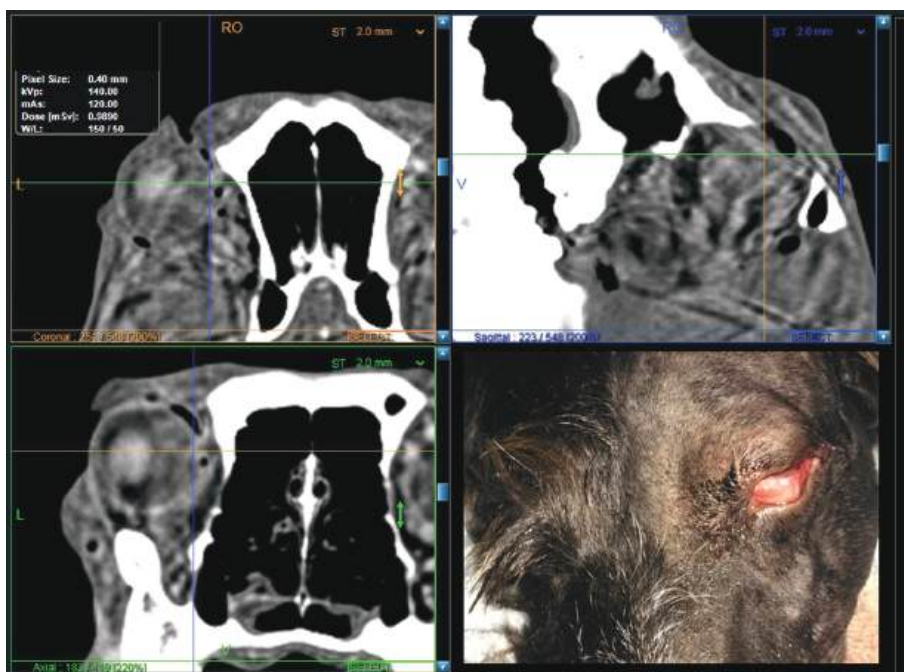

Figure 18. Clinical case 2. Intraoperative CT imaging for case number 2 after removal of the OFBs, and before closure of the soft tissue. Coronal, sagittal and axial sections revealed resolution of the abscess and the eye globe indentation, and no linear structures suspicious of OFBs could be identified. Postoperative appearance after soft tissue closure revealed moderate periocular swelling.

An additional 5 mm opening was left in the conjunctival fornix to allow for the possible drainage of the orbital inflammatory content and decrease the risk of compressive optic neuropathy. Postoperative treatment included continuing previously prescribed amoxicillin with clavulonic acid (13.75 mg/kg BW q12h for 14 days, Zoetis, Parsippany, NJ), oral metronidazole (15 mg/kg BW q12h for 14 days, Unichem Pharmaceuticals, East Brunswick, NJ); oral prednisone (0.5 mg/kg BW q12h for 10 days, then q24h for 10 days, then q48h for 10 days, Jubilant Cadista Pharmaceuticals Inc. Salisbury, MD); oral tramadol hydrochloride (3 mg/kg BW q12h for 14 days, Sun Pharmaceuticals, Cranbury, NJ), oral maropitant (Cerenia 2.2 mg/kg q24h for 5 days, Zoetis, Parsippany,

NJ) and topical Neopolybac QID OS (Bausch and Lomb, Vaughan, ON, CA). The e-collar and exercise restriction (leash walks only) were recommended for 14 days. The checkup examination with a referring ophthalmologist was performed 14 days after surgical procedure and reported visual left eye, with the presence of a focal chorioretinal scar in the ventral inferior fundus corresponding to the previous region of the eye globe indentation and the first foreign body location.

Clinical Case 3.

The patient initially presented with the history of traumatic head injury four days prior, hyphema (1+), vitreal hemorrhage (3+) and traumatic retinal detachment in the left eye resulting in the blindness but still present dazzle response and pupil light reflex with blue light illumination, but absent pupil light reflex with red light illumination (cPLR Tester, Vision Biomedical Solutions, Apatin, Serbia). The right eye was visual, and did not have any abnormalities At the time of the initial examination, systemic (oral prednisone 0.5 mg/kg BW q12h, Jubilant Cadista Pharmaceuticals Inc. Salisbury, MD), and topical steroid (dexamethasone sodium phospate 0.1% q6h OD, Bausch and Lomb, Vaughan, ON, CA) were initiated with the goal of clearing the blood from the eye and preparing the patient for vitreo-retinal surgery. Preoperative glaucoma screening revealed open angle conformation with normal pectinate ligament structure using the gonioscopy with Koeppe lens (Ocular Instruments, Irvine, CA), while the high frequency ultrasound evaluation using the 35 MHz probe (Reichert Inc, Buffalo, NY) revealed collapsed cleft indicative of the hereditary glaucoma predisposition (open angle-closed cleft conformation). One month after the initial presentation to our hospital, a standard pars plana vitreo-retinal re-attachment procedure was pursued with PFO-silicone oil exchange with the continuation of the postoperative anti-inflammatory therapy using systemic and topical steroids as initiated preoperatively, initiation of systemic antibiotic (enrofloxacin 7 mg/kg BW q24h for 14 days, Dechra, Overland Park, KS) and pain medications (tramadol 3 mg/kg BW q12h for 14 days, Sun Pharmaceuticals, Cranbury, NJ). Topical anti-glaucoma medications (latanoprost 0.005% q24h OS Bausch and Lomb, Vaughan, ON, CA and dorzolamide HCl q12h OD, Sandoz Inc, Princteon, NJ) and topical tacrolimus 0.03% (q6h OS, Stokes Pharmacy, Mt Laurel Township, NJ) were initiated. The first recheck examination was performed one week after vitreo-retinal surgery and it revealed a comfortable left eye, with normal intraocular pressure and no evidence of active intraocular inflammation. Two weeks after vitreo-retinal surgery the owner reported ocular discomfort and swelling in the left eye, and an emergency ophthalmology examination was performed which revealed elevated intraocular pressure in the left eye (38 mmHg), with miotic pupil and possible posterior synechiae formations and active intraocular inflammation (flare 1+). Moderate periocular and eyelid swelling was present on ophthalmological examination. Four rounds of topical mydriatics were pursued to dilate the pupil (phenylephrine 2.5% TID OD, tropicamide 1% TID OD, Akorn, Gurnee, IL), which resulted in a moderate pupil dilatation and acute intraocular pressure spike to 58

mmHg indicative of the positive provocative test confirming the diagnosis of primary glaucoma. There were no abnormalities observed in the right eye. Four rounds of topical latanoprost and dorzolamide were initiated every 15 minutes for 1 hour, which resulted in the IOP reduction to 26 mmHg. Treatment was continued with systemic and topical steroids, and latanoprost+dorzolamide eye drops (q8h OS). One week later a follow up checkup was pursued, during which IOP OS was elevated at 37 mmHg with iris bombae formation and presence of active uveitis (2+ flare). More prominent periocular and eyelid swelling was present, with pain during the globe retropulsion and mouth opening. Due to the presence of severe ocular discomfort, uncontrolled glaucoma, uncontrolled intraocular and periocular inflammation and blindness, we have discussed with the client to pursue surgical removal of the left eye combined with iCT imaging. The iCT imaging was proposed due to the concerns about possible retrobulbar pathology (tumor, abscess, cellulitis, endophthalmits/panophthalmitis). Surgical removal of the left eye was routinely performed, and the eye globe, eyelid and orbital tissue were submitted for histopathology analysis. During the enucleation procedure, pockets of subconjunctival silicone accumulation were identified at the sites of previous 23g trocar placements (Figure 19).
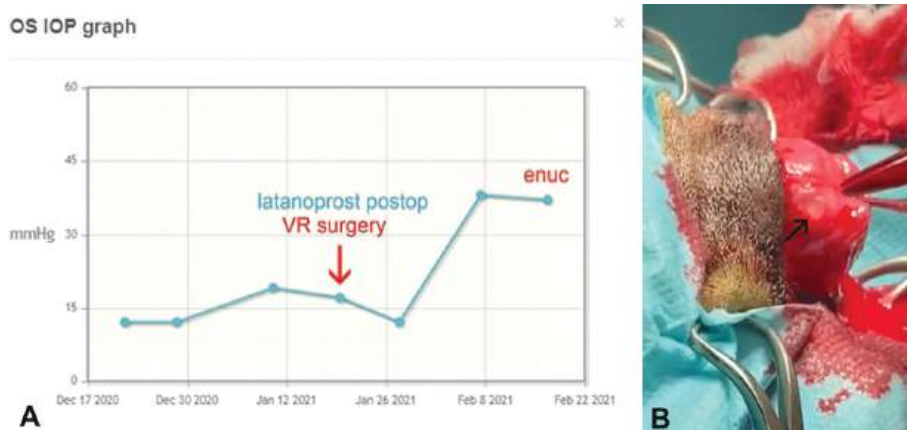

Figure 19. Clinical case 3. (A) Intraocular pressure (IOP) curve in this patient before and after surgery. **(B)** Intraoperative photo during the enucleation procedure reveals the subconjunctival blob with the silicone accumulation at the site of the previous pars plana trocar placement for the vitreo-retinal surgery.

Intraoperative CT was performed and it revealed a focal increase in radiodensity in the eyelids identical to the radiodensity of the silicone prosthesis, potentially indicative of silicone diffusion in the eyelid structures, so the suspicion of a possible silicone oil inflammatory reaction was established (Figure 20). The decision was made to leave the silicone prosthesis in place to achieve a better cosmetic outcome, with the plan to pursue the removal of the silicone prosthesis in the case of a continuous ongoing inflammatory reaction. Postoperative treatment was initiated using oral enrofloxacin

(8 mg/kg BW q24h for 14 days, Dechra, Overland Park, KS), carprofen (Rimadyl, 2.2 mg/kg BW q12h for 14 days, Zoetis, Parsippany, NJ), and tramadol (3 mg/kg BW q12h for 14 days, Sun Pharmaceuticals, Cranbury, NJ). Preventative anti-glaucoma medication was continued in the right eye (latanoprost 0.005% q24h OS Bausch and Lomb, Vaughan, ON, CA). Histopathology evaluation revealed the presence of a lymphocytic-plasmocytic inflammation of the uvea, eyelids (blepharitis) and orbital soft tissue. Follow-up examinations over eighteen months showed a complete resolution of inflammatory skin and orbital changes and no evidence of active glaucoma in the left eye.
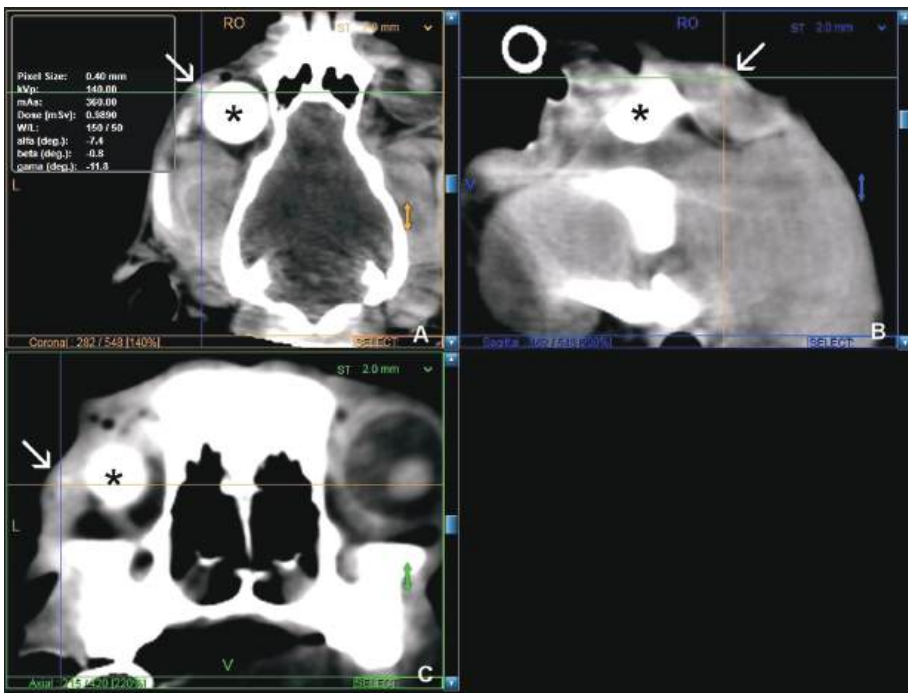

Figure 20. Clinical case 3. Detection of the radiopaque material in the eyelid tissue potentially indicative of the silicone oil migration in the coronal **(A)**, sagittal **(B)** and axial **(C)** scans marked by an arrow. Surgical implant (orbital silicone prosthesis) is clearly visible on the scan (black star).

DISCUSSION

Orbital foreign bodies (OFBs) are any objects originating from an external source that become lodged within the orbit. These foreign bodies can cause serious complications such as infection, inflammation, damage to surrounding tissues, and even vision loss. Timely and accurate detection, localization, and removal of these foreign objects are crucial for preserving vision and overall health [14-18].

Several studies have successfully utilized *in vitro* skull models to evaluate sensitivity and specificity of CT and MRI for detecting different OFBs, with the aim of improving the clinical diagnostics [13,19,20]. This study adopted a similar approach intending to provide additional information on the sensitivity of OFBs detection specific to canine orbital anatomy. Additionally, the observed difference in the detection rate between novice and experienced examiners, further underscores the need for more structural education for veterinary ophthalmologists in CT image analysis, especially in intraoperative situations.

Previous studies have shown that X-ray imaging is often the first choice for imaging foreign bodies due to its widespread availability, relatively low cost, and rapid results [21-23]. Conventional plain radiographs are useful for detecting radiopaque materials such as metal, glass, and some types of plastic. However, radiolucent materials like wood and organic tissues are undetectable by x-rays. Computed tomography (CT) overcomes many of the limitations of plain radiography by providing cross-sectional images and three-dimensional reconstructions of the orbit. CT scans are more sensitive to a wider range of foreign body materials and can determine the precise location and size of objects. Nevertheless, CT scans expose patients to higher radiation doses and have low to moderate sensitivity for the detection of wood-based OFBs, as also confirmed by this study [9,14-16,19,20].

Ultrasound imaging is a non-invasive, portable, and radiation-free diagnostic tool that uses high-frequency sound waves to produce real-time, dynamic images of orbital structures for diagnostic and surgical purposes [24,25]. Ultrasound is particularly useful for localizing non-radiopaque foreign bodies like wood or organic materials, not easily seen on CT scans, as demonstrated in some of the clinical cases described in this study [26-28]. Although ultrasound has a lower spatial resolution compared to CT, it can be deployed faster intraoperatively and costs less than CT imaging [27-29]. However, variations in operator skill and experience may affect the quality of the ultrasound image based diagnostic capability, and two-dimensional images potentially limits the stereotaxic utilization of surgical approach to the orbit [30-32].

While magnetic resonance imaging (MRI) is another advanced imaging technology that has shown the high sensitivity and specificity for detection of orbital pathology and orbital foreign bodies, it has significant limitations. It is contraindicated for patients with metallic implants or ferromagnetic materials as OFBs, as the strong magnetic forces can cause these objects to move or heat up, potentially causing injury [33]. MRI is more expensive, time-consuming, and less accessible for intraoperative imaging compared to other modalities.

This is the first study to demonstrate a feasible approach for the stereotaxic navigation CT-based orbital surgical approach tailored to canine orbital anatomy. The *in vitro* study results showed good reproducibility of the stereotaxic approach, however the real value of this technology will need to be validated during actual clinical application in live patients. Different studies showed the feasibility of the endoscopic orbital

approach for inspecting the canine orbit, aiming to avoid a more invasive type of orbital surgery [34-36]. This study demonstrated that a combination of preoperative and intraoperative CT (iCT), along with ultrasound imaging and endoscopic orbital inspection, can be effectively used for the OFB removal, thus circumventing the traditional lateral zygomatic approach as previously reported [26]. While previous case reports described a silicone orbital prosthesis allergic reaction in a dog [37], this is the first study to report a suspected silicone oil induced blepharitis and cellulits, as previously reported in human patients after vitreo-retinal surgery [38].

This study suggests that the possible use of iCT for canine orbital procedures holds potential, potentially offering less traumatic and more elegant diagnostic and surgical solutions compared to the radical zygomatic approach commonly used in veterinary medicine.

CONCLUSION

Intraoperative CT orbital imaging has the potential to revolutionize the way veterinary ophthalmologists and surgeons approach complex orbital surgery by providing real-time, high-resolution visualization of the surgical field, particularly when combined with stereotaxic navigation surgery. This innovative technology can improve the safety and effectiveness of surgery while reducing the need for reoperations. Despite the challenges and limitations, iCT imaging is likely to become an increasingly valuable tool in the surgical management of orbital conditions, ultimately improving patient outcomes and care quality in veterinary ophthalmology.

Authors' contributions

SG designed the study, performed data analysis, and helped with manuscript preparation, HM performed in vitro CT experiments, TL performed data analysis and helped with manuscript preparation, SL performed data analysis and helped with manuscript preparation, SDJ performed data analysis and helped with manuscript preparation, DS designed and performed in vitro navigation study, performed data analysis and helped with manuscript preparation, DB performed in vitro navigation study and helped with manuscript preparation.

Declaration of conflicting interests

The authors declared no potential conflicts of interest with respect to the research, authorship, and/or publication of this article.

Statement of Informed Consent

The owner understood procedure and agrees that results related to investigation or treatment of their companion animals, could be published in Scientific Journal Acta Veterinaria-Beograd.

ORCID iDs

Siniša D. Grozdanić ⬤ https://orcid.org/0000-0002-9892-3289

REFERENCES

1. Nazimi AJ, Khoo SC, Nabil S, Nordin R, Lan TH, Rajandram RK, Rajaran JR: Intraoperative Computed Tomography Scan for Orbital Fracture Reconstruction. J Craniofac Surg 2019, 30(7):2159-2162.

2. Terpolilli NA, Rachinger W, Kunz M, Thon N, Flatz WH, Tonn JC, Schichor C: Orbit-associated tumors: navigation and control of resection using intraoperative computed tomography. J Neurosurg 2016, 124(5):1319-1327.

3. Sharma P, Rattan V, Rai S, Chhabbra R: Does intraoperative computed tomography improve the outcome in zygomatico-orbital complex fracture reduction? J Maxillofac Oral Surg 2021, 20(2):189-200.

4. Karcioglu ZA, Mascott CR: Computer-assisted image-guided orbit surgery. Eur J Ophthalmol 2006, 16(3):446-452.

5. Klimek L, Mösges R, Laborde G, Korves B: Computer-assisted image-guided surgery in pediatric skull-base procedures. J Pediatr Surg 1995, 30(12):1673-1676.

6. Sandeman DR, Gill SS: The impact of interactive image guided surgery: the Bristol experience with the ISG/Elekta viewing Wand. Acta Neurochir Suppl 1995, 64:54-58.

7. Zhao Y, Li Y, Li Z, Deng Y: Removal of orbital metallic foreign bodies with image-guided surgical navigation. Ophthalmic Plast Reconstr Surg 2020, 36(3):305-310.

8. Yao Q, Wu HP, Xiong B, Han P, Zheng CS: A new method of 3-dimensional localization of intraocular foreign bodies using CT imaging: A role of optic nerve. J Huazhong Univ Sci Technolog Med Sci 2017, 37(1):110-114.

9. You Y, Wang X, Cheng S, Zhu R, Wang B, Li S, Jiang F: Clinical analysis of 96 patients with intraorbital foreign bodies: A 10-year retrospective study. Front Med (Lausanne) 2022, 9:1018905.

10. Marcus H, Schwindack C, Santarius T, Mannion R, Kirollos R: Image-guided resection of spheno-orbital skull-base meningiomas with predominant intraosseous component. Acta Neurochir (Wien) 2013; 155(6):981-988.

11. Servat JJ, Elia MD, Gong D, Manes RP, Black EH, Levin F: Electromagnetic image-guided orbital decompression: technique, principles, and preliminary experience with 6 consecutive cases. Orbit 2014, 33(6):433-436.

12. Aras MH, Miloglu O, Barutcugil C, Kantarci M, Ozcan E, Harorli A: Comparison of the sensitivity for detecting foreign bodies among conventional plain radiography, computed tomography and ultrasonography. Dentomaxillofac Radiol 2010, 39(2):72-78.

13. Javadrashid R, Golamian M, Shahrzad M, Hajalioghli P, Shahmorady Z, Fouladi DF, Sadrarhami S, Akhoundzadeh L: Visibility of different intraorbital foreign bodies using plain radiography, computed tomography, magnetic resonance imaging, and cone-beam computed tomography: an *In vitro* study. Can Assoc Radiol J 2017; 68(2):194-201.

14. Jusue-Torres I, Burks SS, Levine CG, Bhatia RG, Casiano R, Bullock R: Wooden foreign body in the skull base: how did we miss it? World Neurosurg 2016, 92:580 e5 – e9.

15. Kim YH, Kim H, Yoon ES: Unrecognized intraorbital wooden foreign body. Arch Craniofac Surg 2018, 19(4):300-303.

16. Pandit K, Sitaula S, Shrestha GB, Joshi SN, Chaudhary M: Management of unusual missed diagnosis of a Intra-orbital wooden foreign body: A case report and review of literature. Ann Med Surg (Lond) 2022, 79:104017.

17. Singh P, Desai A, Das D, Bajaj MS: Large wooden orbital foreign body: case report and literature review. Trop Doct 2021, 51(2):235-237.

18. You YY, Shi BJ, Wang XY, Chen J, Wang ZR, Wang XH, Jiang FG: Intraorbital wooden foreign bodies: case series and literature review. Int J Ophthalmol 2021, 14(10):1619-1627.

19. Ayalon A, Fanadka F, Levov D, Saabni R, Moisseiev E: Detection of intraorbital foreign bodies using magnetic resonance imaging and computed tomography. Curr Eye Res 2021, 46(12):1917-1922.

20. McGuckin JF, Jr., Akhtar N, Ho VT, Smergel EM, Kubacki EJ, Villafana T: CT and MR evaluation of a wooden foreign body in an *in vitro* model of the orbit. AJNR Am J Neuroradiol 1996, 17(1):129-133.

21. Markowski J, Dziubdziela W, Gierek T, Witkowska M, Mrukwa-Kominek E, Niedzielska I, Paluch J: Intraorbital foreign bodies—5 own cases and review of literature. Otolaryngol Pol 2012, 66(4):295-300.

22. Murphy KJ, Brunberg JA: Orbital plain films as a prerequisite for MR imaging: is a known history of injury a sufficient screening criterion? AJR Am J Roentgenol 1996, 167(4):1053-1055.

23. Williamson MR, Espinosa MC, Boutin RD, Orrison WW, Jr., Hart BL, Kelsey CA: Metallic foreign bodies in the orbits of patients undergoing MR imaging: prevalence and value of radiography and CT before MR. AJR Am J Roentgenol 1994, 162(4):981-983.

24. Cirla A, Rondena M, Bertolini G: Automated tru-cut imaging-guided core needle biopsy of canine orbital neoplasia. A prospective feasibility study. Open Vet J 2016, 6(2):114-120.

25. Flaherty EH, Robinson NA, Pizzirani S, Pumphrey SA: Evaluation of cytology and histopathology for the diagnosis of canine orbital neoplasia: 112 cases (2004-2019) and review of the literature. Vet Ophthalmol. 2020, 23(2):259-268.

26. Grahn BH, Szentimrey D, Pharr JW, Farrow CS, Fowler D: Ocular and orbital porcupine quills in the dog: a review and case series. Can Vet J 1995, 36(8):488-493.

27. Close JK, Shiels WE, 2nd, Foster JA, Powell DA: Percutaneous ultrasound-guided intraorbital foreign body removal. Ophthalmic Plast Reconstr Surg 2009, 25(4):335-337.

28. Patel SH, Bakhsh S, Badar A, Hajrasouliha AR: Ultrasound biomicroscopy and echogenic external marker assisted intraocular foreign body removal. Retin Cases Brief Rep 2024, 18(1):29-31.

29. Abu-Zidan FM, Balac K, Bhatia CA: Surgeon-performed point-of-care ultrasound in severe eye trauma: Report of two cases. World J Clin Cases 2016, 4(10):344-350.

30. Stades FC, Djajadiningrat-Laanen SC, Boroffka SA, Boeve MH: Suprascleral removal of a foreign body from the retrobulbar muscle cone in two dogs. J Small Anim Pract 2003, 44(1):17-20.

31. Hartley C, McConnell JF, Doust R: Wooden orbital foreign body in a Weimaraner. Vet Ophthalmol 2007, 10(6):390-393.

32. Tremolada G, Milovancev M, Culp WT, Bleedorn JA: Surgical management of canine refractory retrobulbar abscesses: six cases. J Small Anim Pract 2015, 56(11):667-670.

33. Ghemame M, Cathelineau C, Carsin-Nicol B, Eliat PA, Saint-Jalmes H, Ferre JC, Mouriaux F: Ex vivo porcine model for eye, eyelid, and orbit movement analysis of 4-mm ferromagnetic foreign bodies in MRI. Graefes Arch Clin Exp Ophthalmol 2022, 260(1):311-318.

34. Braunstein RE, Kazim M, Schubert HD: Endoscopy and biopsy of the orbit. Ophthalmic Plast Reconstr Surg 1995, 11(4):269-272.

35. Espinheira Gomes F, Porter I, Sumner JP: Transorbital postcaruncular endoscopic surgery as an alternative to orbital exploratory surgery: A cadaveric study and case report in a dog with an orbital sarcoma. Vet Surg 2020, 49(7):1359-1366.

36. Djuric ML, Krstic VP, Lazic TM, Grozdanic SD: Endoscopic diagnostic and surgical orbital approach in canines. Acta Vet Hung 2022.

37. Muramatsu Y, Fukushima U, Kudo S, Akatsuka T, Ono K, Hirao H: Silicone allergy associated with intraocular silicone ball prosthesis in a dog. Can Vet J 2021, 62(11):1185-1189.

38. Lemaitre S, Vahdani K, Escalas P, Rose GE: Orbital leakage of intraocular silicone oil: case reports and literature review. Ophthalmic Plast Reconstr Surg 2020, 36(3):e75-e8.

UPOTREBA KOMPJUTERSKE TOMOGRAFIJE ZA PREOPERATIVNU I INTRAOPERATIVNU IDENTIFIKACIJU ORBITALNIH STRANIH TELA I PLANIRANJE HIRURŠKOG PRISTUPA U VETERINARSKOJ MEDICINI

Siniša D. GROZDANIĆ, Heidi MURTHA, Tatjana LAZIĆ, Slavica ĐUKIĆ, Sergei LUZETSKII, Daniel C. URSU, David SARMENT

Cilj ove studije bio je da se proceni osetljivost intraoperativnog kompjuterizovanog tomografskog (iCT) snimanja za detekciju stranih tela u orbiti (OFB) u *in vitro* modelu i da se proceni efikasnost iCT-a u planiranju hirurškog uklanjanja OFB-a kod veterinarskih pacijenata. U našu bolnicu dovedena su tri psa zbog mogućeg uklanjanja stranog tela iz orbite. *In vitro* studije su sprovedene koristeći model lobanje psa sa postavljanjem različitih OFB-ova. Četiri različita ispitivača su koristila CT snimanje kako bi procenili detekciju OFB-a. Hirurški navigacioni sistem je korišćen kako bi se procenila izvodljivost stereotaktičkog uklanjanja stranih tela iz orbite *in vitro*. iCT snimanje je primenjeno za planiranje i vođenje hirurškog zahvata uklanjanja OFB-a kod tri klinička pacijenta. *In vitro* eksperimenti su pokazali visoku stopu detekcije objekata sa visokom

radiopacitetom, kao što su metal i staklo. Stopa detekcije organskih stranih tela, kao što je drvo, bila je umerna, dok je za plastične strane predmete varirala od umerne do niske. Navigacija je uspešno korišćena za vađenje OFB-a. iCT je efikasno primenjen za detekciju OFB-a kod kliničkih pacijenata. Međutim, šiljci od ježa su bolje detektovani standardnim ultrazvučnim snimanjem. Upotreba iCT-a potencijalno predstavlja evoluirajuću tehnološku praksu koja omogućava realno vreme snimanja radi poboljšanja preciznosti hirurških postupaka.